Third-harmonic generation in the presence of classical nonlocal effects in gap-plasmon nanostructures

Cristian Ciracì, Michael Scalora, and David R. Smith

Phys. Rev. B **91**, 205403 — Published 8 May 2015

DOI: 10.1103/PhysRevB.91.205403

Third-Harmonic Generation in the Presence of Classical Nonlocal Effects in Gap-Plasmon Nanostructures

Cristian Ciracì,[1,*] Michael Scalora,[2] and David R. Smith[3]

[1] *Istituto Italiano di Tecnologia (IIT), Center for Biomolecular Nanotechnologies, Via Barsanti, 73010 Arnesano, Italy.*
[2] *C.M. Bowden Research Facility, US Army, RDECOM, Redstone Arsenal, AL 35803, U.S.*
[3] *Center for Metamaterials and Integrated Plasmonics, and Departement of Electrical and Computer Engineering, Duke University, Durham NC 27708, U.S.*

(Dated: April 20, 2015)

Classical nonlocality in conducting nanostructures has been shown to dramatically alter the linear optical response, by placing a fundamental limit on the maximum field enhancement that can be achieved. This limit directly extends to all nonlinear processes, which depend on field amplitudes. A numerical study of third-harmonic generation in metal film-coupled nanowires reveals that for sub-nanometer vacuum gaps the nonlocality may boost the effective nonlinearity by five orders of magnitude as the field penetrates deeper inside the metal than that predicted assuming a purely local electronic response. We also study the impact of a nonlinear dielectric placed in the gap region. In this case the effect of nonlocality could be masked by the third harmonic signal generated by the spacer. By etching the dielectric underneath the nanowire however it is possible to muffle such contribution. Calculations are performed for both silver and gold nanowire.

PACS numbers: 0000000

I. INTRODUCTION

Large optical nonlinearities are critical to photonic technologies. The exploitation of nonlinear processes at low power levels, and in highly integrated formats, requires materials with large nonlinear susceptibilities in configurations that offer efficient nonlinear conversion. Metals have long been recognized as compelling candidates for nonlinear materials, as they possess nonlinear susceptibilities that are orders of magnitude larger than dielectric materials, and support surface plasmon modes that allow the light to become strongly confined and enhanced in deeply sub-wavelength volumes. As a result, a major research effort has been targeted toward metal-dielectric composites[1,2], including metallo-dielectric stacks[3–5], metamaterial composites[6–10], structured films[11,12] and surfaces[13–15]. While the absorption inherent to metals is generally considered to be detrimental for linear applications, it is far less critical for nonlinear optical applications because conversion rates are expected to be smaller than a fraction of a percent.

Although metals possess large nonlinearities, their high reflectivity has hindered their adoption as nonlinear optical materials. Even though metals may generally be opaque and highly reflective, metal nanostructures with features much smaller than the incident wavelength can interact strongly with light. For example, recent works on structured metallic absorbers have shown that reflectivity and other optical characteristics can be modified substantially. Structured nanoparticles, such as crosses, disks, or rods, deposited on a dielectric spacer atop a metal substrate can introduce an effective magnetic response that can impedance-match the surface to the vacuum, thus minimizing reflections and maximizing absorption[16–18].

In most key optical applications of metals, the nanoscale gaps between coupled metallic nanostructures are critical, with smaller gaps increasing local field enhancement and confinement. As gap size decreases to sub-nanometer scales, two basic issues must be dealt with: i) the conventional local description of the electronic response of strongly coupled metal nanoparticles breaks down, as the the dielectric constant of the metal acquires a wave-vector dependence; and ii) induced quantum currents turn the vacuum into a conductor as a result of quantum tunneling. In linear systems, the effect of classical nonlocality in gold-based film-coupled nanoparticles can limit the achievable field enhancement[19]. The influence of quantum mechanical effects, in which electron tunneling reduces field enhancement in the gap region, has been investigated both theoretically[20–22] and experimentally[23–25]. In the *extreme coupling* regime, all of the models of electron response that extend beyond the local response tend to reduce the expected field enhancements, suggesting that nonlinear processes may also be significantly affected.

In this article we theoretically investigate a configuration where the inclusion of nonlocal effects can dramatically alter the effective nonlinear polarizability of the metal by several orders of magnitude. This occurs because surface charges begin to permeate the volume immediately beneath the surface of the metal, thus allowing the fields to access the large, intrinsic third-order nonlinearity typical of metals. Although this process would affect the overall nonlinear properties of metals, we show that it is possible to enhance the alteration due to the nonlocal free-electron response by employing structures with very small gap region sandwiched between metal layers. In particular we consider metal wire arrays possessing a rectangular cross-section spaced by a metal film via a nanometric dielectric layer. Such structures can be fabricated using atomic layer lithography techniques.

Chen *et al.* have shown that by using atomic layer deposition it is possible to fabricate nanometer-size gaps in metal films that extends several millimeters[26]. These techniques have been used to show third harmonic generation enhancement from gold wires coupled to a gold film[27]. Other authors[25,28] have been investigating similar structures, such as film-coupled circular nanowires[28] and spheres[25]. These structures however usually possess a plasmonic resonance around the center of the visible spectrum, making it impossible to resonate at the fundamental wavelength.

In order to show how nonlocality can affect third-harmonic generation (THG), we employ a simple model in which we separate the contribution of the free-electron polarization, which will be consider nonlocal, from the one due to the inner, *bounded* electrons. In particular, the latter will be responsible for the nonlinear contribution. The model will be outlined in Section II. In section III we will show the effect of considering a nonlocal contribution in the free-electron response rather than a simple local response, showing the this will drastically alter the THG for vacuum gap structures. This oversimplified situation will be extended in section IV by taking into account a more realistic geometrical implementation. In particular we will show the impact of different nobel metals and the impact of a THG contribution rising from the dielectric spacer layer. A possible experiment will be suggested in other to experimentally demonstrate our findings. Conclusions will be drawn in the last section.

II. CLASSICAL MODEL

The complexity of the metal optical response can be described by treating separately the different polarization contributions[29]. Free electrons are able to move around the entire volume, while bound electrons are tied up around their equilibrium position, creating thus two effective polarization surfaces. Let us indicate the thickness of the free-electron shell as δ as depicted in Fig. 1 Quantum calculations based on the jellium model, in which the ionic lattice is described by a uniform positive background charge density, suggest that the effective location of the free-electron surface may be assumed in correspondence of the center of mass of the induced charge density[30,31]. The position of this effective surface depends on the work function of the specific metal and it is usually displaced a good fraction of one angstrom with respect to the jellium edge[21]. While for metals that are well described by the jellium model, like for example sodium, the screening charges are located at approximately at 1 Å outside the jellium edge (i.e. $\delta \simeq$1Å), for silver and gold, experimental data[32–34] seems to suggest that the effect of inner electrons is to push the reach of 5-s (free) electron peak density inside the jellium edge[21]. This would correspond in our model to an overlap of the free and bound electron surfaces ($\delta \simeq 0$). Note that we neglect the typical exponential decay of the electron density outside the effective surfaces and consider instead a *hard wall*-like boundary.

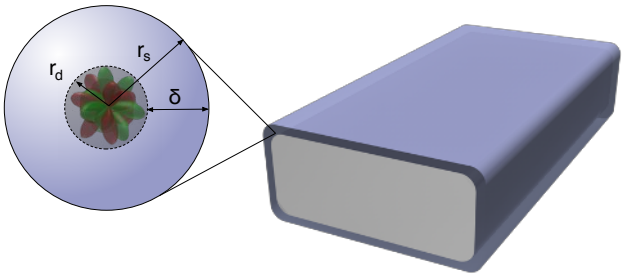

FIG. 1. Effective polarization surfaces. Free-electrons extend over the polarizability volume associated to the bound electrons. The difference can be intuitively associated to the extension of the s-electron orbitals.

The process of third-harmonic generation (THG) can be described by means of the nonlinear wave equation. For an electric field $\mathbf{E}$ oscillating at the angular frequency ω we have:

$$\nabla \times \nabla \times \mathbf{E} - \frac{\omega^2}{c^2}\mathbf{E} = \omega^2 \mu_0 \mathbf{P}, \tag{1}$$

where c is the speed of light in free-space and μ_0 is the magnetic permeably. In Eq. (1), we explicitly write the polarization $\mathbf{P}$ of the medium as a source term. The vector $\mathbf{P}$ is subdivided into three contributions: i) free electron response $\mathbf{P}_{\rm f}$, ii) bound electron response $\mathbf{P}_{\rm b}$ and iii) nonlinear response $\mathbf{P}_{\rm NL}$:

$$\mathbf{P} = \mathbf{P}_{\rm f} + \mathbf{P}_{\rm b} + \mathbf{P}_{\rm NL}. \tag{2}$$

The free-electron portion is treated using the hydrodynamic model, an extension of the Drude model that accounts for the effect of the electron pressure[35]. In particular, the free-electron pressure gives rise to the nonlocal portion of the polarization, and may be determined from the equation:

$$-\beta^2 \nabla \left(\nabla \cdot \mathbf{P}_{\rm f}\right) - \left(\omega^2 + i\omega\gamma\right)\mathbf{P}_{\rm f} = \omega_{\rm p}^2 \varepsilon_0 \mathbf{E}, \tag{3}$$

where $\omega_{\rm p}$ and γ are the plasma frequency and the collision rate, respectively, which also appear in the conventional Drude formula. The parameter β is approximately the speed of sound in the Fermi-degenerate plasma of conduction electrons, that is $\beta^2 = \frac{1}{3} v_F^2$[35].

The portion of the polarization due to the bound electrons is considered in the limit of the local-response approximation and it could be described as a multipole Lorentz oscillator:

$$\mathbf{P}_{\rm b} = \varepsilon_0 \left[-\sum_j \frac{\omega_{{\rm p},j}^2}{\omega^2 - \omega_{0,j}^2 + i\omega\gamma_j} \right] \mathbf{E}, \tag{4}$$

where j is an index labeling the individual d-band to sp-band electron transitions occurring at $\omega_{0,j}$. The nonlinear contribution is a third-order function of the

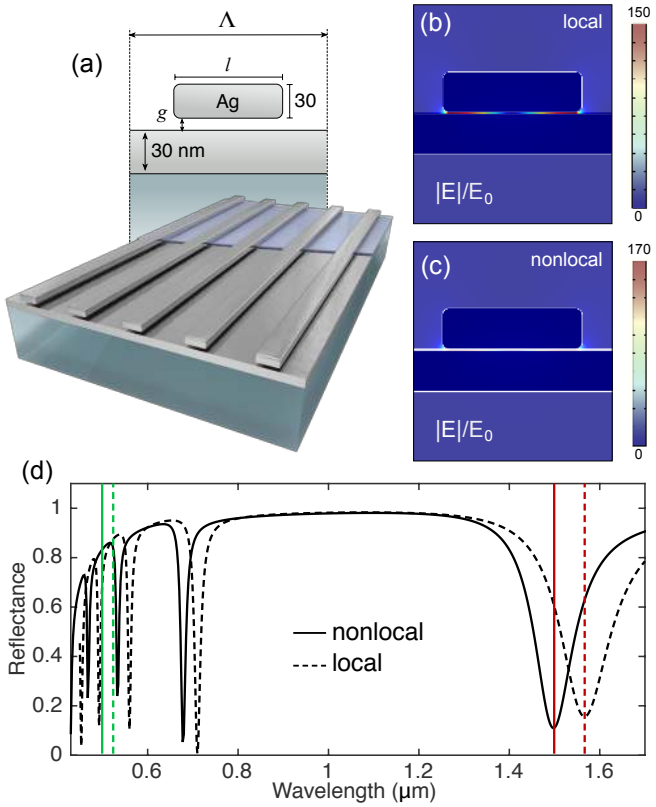

FIG. 2. The film-coupled nanowire system. (a) Schematic of the geometry with array of nanowires coupled to a metal film via a small gap. (b) Cross-section of the electric field distribution from finite-element simulations, displaying the fundamental cavity mode for the local case. (c) Same as in (b) but for the nonlocal case. (d) Linear reflectance of the film-coupled nanowire geometry with $g = 1$ nm, $l = 100$ nm, and $\Lambda = 200$ nm). The refractive index of the substrate is $n = 1.45$. The red vertical lines indicate the wavelength corresponding to the fundamental mode, while the green ones refer to the third harmonic.

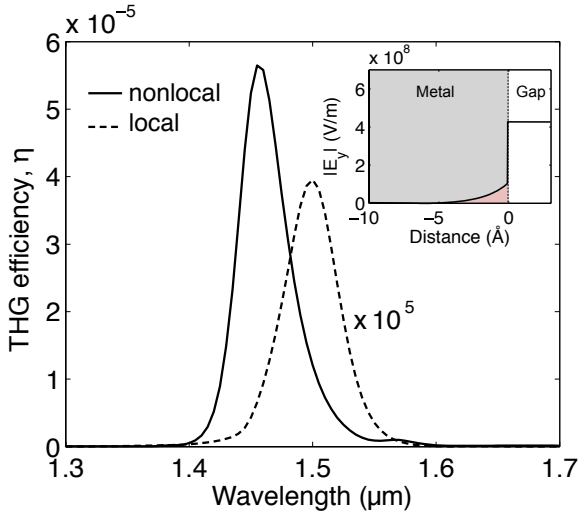

FIG. 3. THG efficiency spectra for the film-coupled nanowire geometry in the case of nonlocal free-electron response (solid line) and local response (dashed line) with $\delta = 0$. The inset shows the electric field amplitude along a line going through the gap in the vicinity of the wire's edge for the nonlocal case. The material parameters used for Ag are: $\beta = 1.26\times10^6$ m/s, $\omega_p = 1.4029 \times 10^{16}$ s^{-1}, $\gamma = 3.0076 \times 10^{13}$ s^{-1}; the permittivity associated with the bound electrons was calculated as the difference between empirical data[39] and the free-electron contribution.

electric fields. For an isotropic material there is only one independent element of the susceptibility tensor $\chi_{ijkl}(3\omega;\omega,\omega,\omega) = \frac{1}{3}\chi^{(3)}(\delta_{ij}\delta_{kl} + \delta_{ik}\delta_{jl} + \delta_{il}\delta_{kj})$ so that the nonlinear polarization can be taken as[36]:

$$\mathbf{P}_{\rm NL} = \varepsilon_0\chi^{(3)}\,(\mathbf{E}\cdot\mathbf{E})\,\mathbf{E} \tag{5}$$

We numerically solve the system of Eqs. (1)-(5) in the undepleted pump approximation, using the finite-element method implemented in the commercially available software COMSOL Multiphysics[37]. Since the equation for the free-electron polarization is nonlocal, an additional set of boundary conditions is needed beyond the well-known tangential field continuity condition. The additional boundary conditions should be applied with some care as bound electrons are assumed to give a local contribution to the polarization vector. Following Ref. 38, we impose that $\mathbf{P}_{\rm f}\cdot\hat{\mathbf{n}} = 0$ at the surface, where $\hat{\mathbf{n}}$ is the unit vector normal to the surface.

We define the THG efficiency in air as the ratio between the third harmonic generated intensity, $I(3\omega)$, over the incident intensity at the fundamental wavelength, $I_0(\omega)$:

$$\eta = \frac{I(3\omega)}{I_0(\omega)}. \tag{6}$$

For simplicity in the rest of the article we will assume an incident intensity of $I_0(\omega) = 50$ MW/cm^2 and a $\chi^{(3)} = 1.0 \times 10^{-18}$ m^2/V^2,[36] if not otherwise specified. Our model has been tested for the simple case of THG from a bare metal film. To obtain a non-zero normal component with respect to the film surface, which allows the fields to access the nonlocal effects, we varied the incidence angle of the pumping field and compared our results to those obtained in the case of the local-response approximation. In absence of nanostructured features the two models completely overlap.

III. THE EFFECT OF NONLOCAL RESPONSE

Let us consider the geometry depicted in Fig. 2a, which consists of an array of infinitely long metallic nanowires with rectangular cross-sections of width l and height 30 nm, and period Λ, separated by a distance g from a metallic film of thickness 30 nm. For simplicity here we assume the surrounding dielectric to be air. A more realistic structure would require a dielectric spacer layer to separate the wires from the metal substrate[40]. The case

of a dielectric nonlinear spacer is reported in Section IV. Each metal nanowire supports a strong resonance whose electric field mode is localized within the cavity formed between the bottom surface of the nanowire and the underlying metal film[18,41], as shown in Figs. 2b and 2c. The reflectivity of the patterned surface can reach values close to zero in correspondence with the peak resonance at normal incidence, as shown in Fig. 2c. In this situation the electric field is squeezed into the gap between the film and the nanowire and locally enhanced in excess of two orders of magnitude with respect to the amplitude of the incident radiation. Figure 3 shows the THG efficiencies for the structure depicted in Fig. 2a, where the metal is assumed to be silver (Ag). The cases in which nonlocal free-electron (NLFE) response and local free-electron response (LFE) is assumed are reported in solid and dashed line respectively. The difference in THG between the local and nonlocal models is enormous. We predict that by including the nonlocal response this geometry will foster an enhancement of THG of more than five orders of magnitude with respect to the local description.

In order to exclude any impact of the periodicity, we appropriately chose a period $\Lambda < \lambda/2$ for the entire spectral region of interest. In this way we avoid higher order scattering, as well as the coupling between grating and plasmic resonances. Each of the resonances in the linear spectra of Fig. 2d corresponds in fact to a higher order gap-plasmon mode[18]. The spectra also show that the quality factor of each resonance does not sensibly change introducing the nonlocality. Moreover, the relative position of between fundamental resonance (red lines) and the third-harmonic resonance (green lines) do not change. In both local and nonlocal cases, the third-harmonic resonance falls in between two resonances: no enhancement can be then attributed to phase-matching improvement. Although, in general, the presence of a nonlocal response has a negative impact on field enhancement, in this specific case the nonlocality improves the local field enhancement as it can be seen form Figs. 2b and 2c. This is due to the fact that nonlocality is affecting the coupling with the incident radiation and in turn compensating for the reduction of field enhancement. This is reflected on the slightly deeper fundamental resonance for the nonlocal case (Fig. 2d). Such difference, however, cannot explain the difference observed in the THG efficiencies. In fact, the field enhancement difference in this case would be responsible for only a factor of $(|E^{nl}_{max}|/|E^{loc}_{max}|)^6 = (170/150)^6 \simeq 2$, far smaller than the 10^5 observed in Fig. 3.

Within the framework of the model adopted, the origin of this striking contrast in THG efficiencies can be associated with the behavior of the conduction electrons, which exhibit different screening properties at the subnanometer scale. The inset of Fig. 3 shows the electric field amplitude on the cross-section along the gap. Although outside the metal region the electric field enhancement is reduced when the nonlocal response is taken into account, the charges are smeared just beneath the metal surfaces, allowing the fields to partially penetrate, reaching portions of the bound and core electrons responsible for the intrinsic third-order nonlinearity.

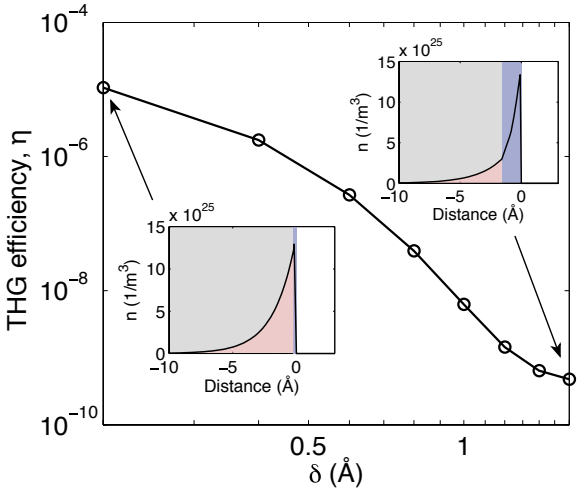

FIG. 4. THG efficiency as a function of the thickness δ of the free-electron-only shell. Calculations were performed assuming $g = 1$ nm, $l = 100$ nm, and $\Lambda = 200$ nm). The THG efficiency peak was plotted in each case. The insets show the induced charge density distribution along a line thorough the gap and in the vicinity of the wire's edge.

Given the surface nature of the phenomenon explored, the hydrodynamic model may not be completely adequate to give an accurate description of the atomic quantum realm. In particular, we have assumed so far that free-electrons are confined inside the exact same boundaries ($\delta = 0$) that delimit the bound electron region. Calculations of THG as a function of the thickness δ of the free-electron shell, as shown in Fig. 4, display a dramatic drop in generation efficiency as δ is increased by a fraction of an angstrom, Fig. 4. The insets show the induced charge density distribution in the vicinity of the metal surface. The scale on which the drop in the THG efficiency occurs may constitute a serious concern to the applicability of the present model, however, we remark that this surface layer does not necessarily have a direct physical counterpart, and it is instead an effective layer associated to the complex interaction between many different electron orbitals.

IV. SILVER, GOLD, AND THE SPACER CONTRIBUTION

The metal linear nonlocal response seems to have a huge impact on the amount of third-harmonic signal generated. It is interesting then to explore the case in which the metal dielectric function is changed. To do so we simply consider the structure to be made of a different material, for example gold (Au). Linear properties of Au are described using the parameters of Ref. 42. Figure 5

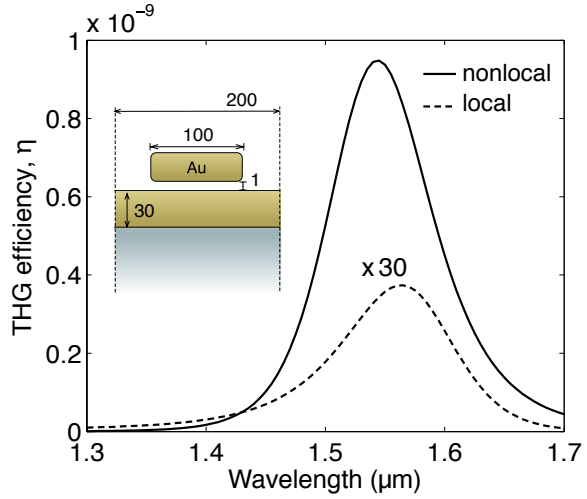

FIG. 5. THG efficiency spectra for the film-coupled nanowire geometry depicted in the inset for nonlocal free-electron response (solid line) and local response (dashed line) with $\delta = 0$. The material parameters used for Au were taken from Ref. 42 with $\beta = 1.26 \times 10^6$ m/s.

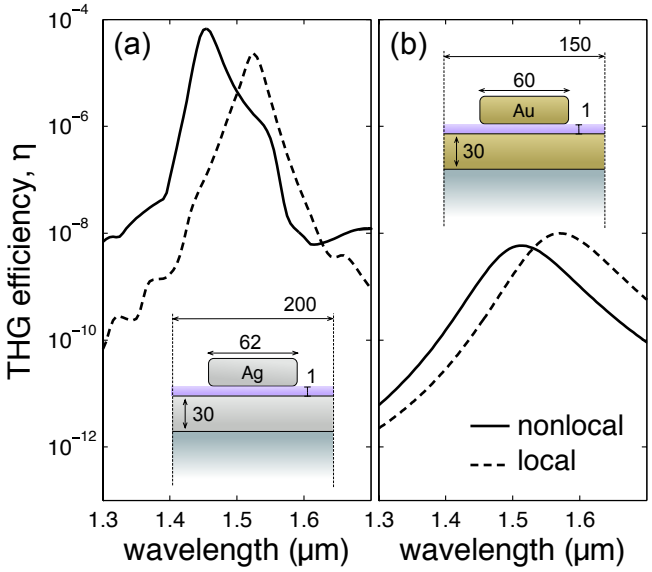

FIG. 6. THG efficiency spectra for the film-coupled nanowire geometry depicted in the insets for nonlocal free-electron response (solid line) and local response (dashed line) in case of Ag (a) and Au (b); the spacing layer was assumed to be Al_2O_3 with refractive index $n = 1.6$ and third order susceptibility $\chi^{(3)} = 1.0 \times 10^{-21}$ m^2/V^2. Geometrical parameters are shown in the insets in nanometers.

shows the THG efficiencies in the case of Au wires coupled to a Au film as depicted in the inset. As in the Ag case (Fig. 3) there is still a difference in the THG efficiencies calculated in the NLFE and LFE cases. However, this time the difference is much more contained. This is due to gold interband transitions that increase absorption about the third harmonic frequency. The excess of THG is re-absorbed by the material itself, generating a reduced effect compared to that obtained for Ag. Since the metal dielectric function seems to be very important, in what follow we will constantly report the two cases of silver and gold.

So far we assumed that the gap between the wires and the film was filled by air. This assumption however may not reflect the fabrication requirement, which in general may require adding a dielectric spacing layer on top of the metal film. In particular we consider that the spacing material is Al_2O_3 similarly to the case of Ref. 27 where similar structures where fabricated using atomic layer lithography. For simplicity we consider a dispersionless material with refractive index $n = 1.6$. We also assume that the material posses an intrinsic $\chi^{(3)}$ which is taken three orders of magnitude smaller than that of the metal, namely $\chi^{(3)}_{Al_2O_3} = 1.0 \times 10^{-21}$ m^2/V^2.[36]

Although the presence of a dielectric spacer does not alter the physics of the structure, the presence of a secondary nonlinear source may make it impossible to distinguish between the two models. In fact, even if the Al_2O_3 possesses an intrinsic $\chi^{(3)}$ much smaller than that of the metal, its nonlinearity is more accessible for the specific geometry considered. Figure 6 shows the THG efficiency spectra for Ag and Au wires spaced by a uniform layer of Al_2O_3 in the case of NLFE and LFE. Using either of the models the amount of third harmonic generated signal is comparable, which would make it hard in an actual experiment to determine any contribution due to the NLFE response[27].

In order to reduce the contribution from the spacer one may think to use simply a dielectric spacer with a even smaller $\chi^{(3)}$, however Al_2O_3 already possesses one of the smallest nonlinear susceptibilities. To overcome this issue then, one has to reduce the amount of dielectric material in the region where the electric field is higher. By looking at Fig. 2b, it is clear that one should preferentially remove the dielectric near the corners of the base of the wires. In principle this can be achieved by etching the Al_2O_3. In Fig. 7 is shown the THG efficiency spectra for Ag and Au wires spaced by a etched layer of Al_2O_3 in the case of NLFE and LFE. In this case the difference between the two models become again visible, for both Ag and Au.

The enhancement introduced by the nonlocal response depends on how much the fields are squeezed near the metal surface. A confirmation of this is the fact that for a bare metal film there is no effect. In order to demonstrate this dependance, we perform calculations of THG as a function of the nanowire distance from the film. The THG efficiencies η for both local and nonlocal cases respectively, are calculated for several values of g and plotted in Figs. 8a and 8b for Ag and Au respectively. However, one should be mindful of the fact that as g increases the resonance blue-shifts, pushing the THG field into the UV range. In the insets of Figs. 8a and 8b we plot the linear absorption as a function of the parameters l and g, keeping the wavelength of the pumping field constant

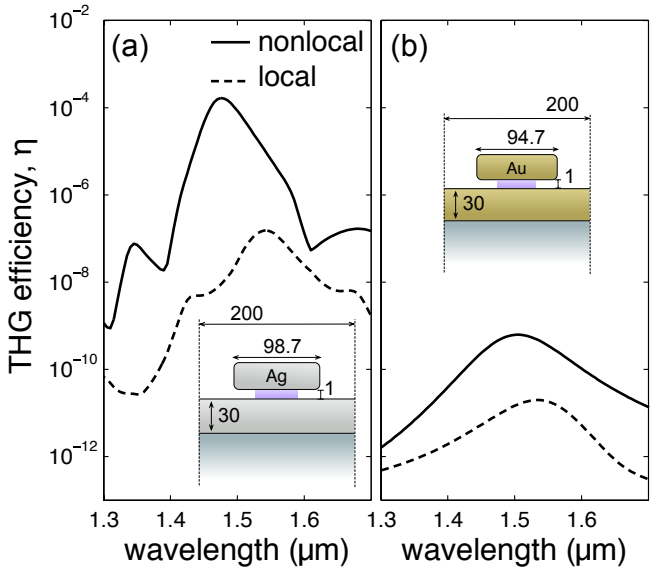

FIG. 7. THG efficiency spectra for the *etched* geometry depicted in the insets for nonlocal free-electron response (solid line) and local response (dashed line) in case of Ag (a) and Au (b). Geometrical parameters are shown in the insets in nanometers. The etching was taken equal to 35 nm.

and equal to $\lambda_{\rm FF} = 1.55\mu$m. The red curve represents the region where the absorption (reflectance) is a maximum (minimum) in the case of NLFE response. The analogous curve was calculated for the local response approximation. For large gaps, the efficiencies are of the same order of magnitude, meaning that the impact of the nonlocality is negligible. However, the effect of the nonlocal free-electron response becomes dominant as the gap closes, generating an enhancement of the THG process of about one order of magnitude over that obtained from the local model.

V. CONCLUSION

The impact of nonlocal linear response on nonlinear properties of metallic nanostructure could be the key to enhance nonlinear optical processes at the nanoscale. We have presented a detailed analysis of such an effect using a rather simple model. Although the hydrodynamic model used to describe the nonlocal response of free-electrons is not entirely adequate to give a correct quantum description of the subatomic realm, its simplicity enables qualitative and quantitative predictions for systems where a full-quantum approach is prohibitive. For example, in physical systems, the geometrical dimensions may exceed several hundreds of nanometers, making the computational domain for quantum calculations prohibitive. Another promising approach could be the generalization of the hydrodynamic model to take into a account a more sophisticated description of the free-electron gas internal energy[43]. Such a description would be more adequate

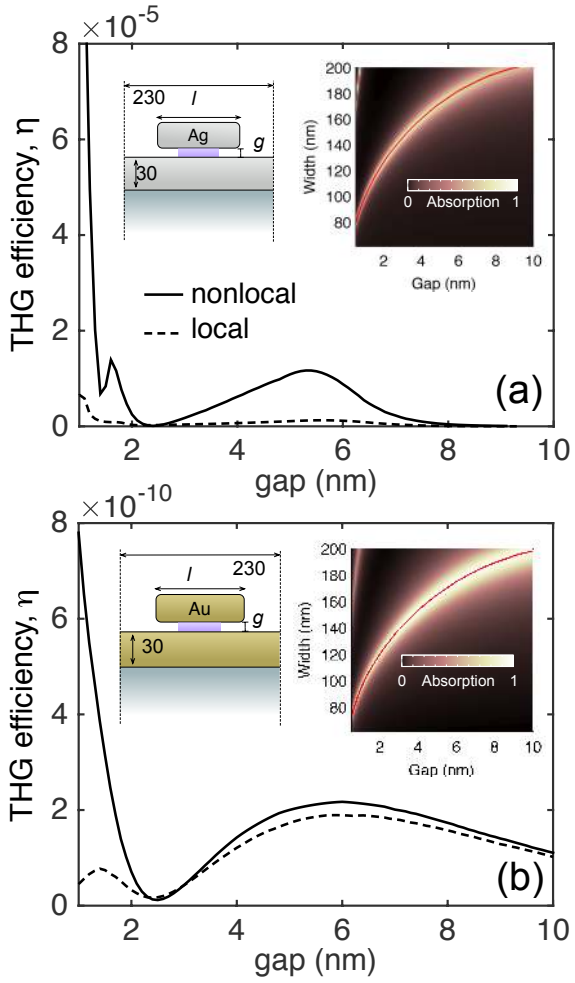

FIG. 8. THG efficiencies are plotted as a function of the distance from the metal substrate. The different curves are obtained using the local-response (dashed) approximation and the hydrodynamic model for free-electrons (solid), respectively for both silver (a) and gold (b). A cross-section of the structure is depicted in the left insets; lengths are expressed in nanometers. The right insets show the absorption map for the film-coupled nonowire system as a function of the parameters l and g for a constant wavelength $\lambda = 1.55\mu$m and period $\Lambda = 230$ nm. The maximum absorption region is outlined by the red curve. The etching was taken fixed at 30 nm.

to describe surface phenomena and at the same time it could be applied to macroscopical systems.

Notwithstanding, we have investigated a variety of different configurations taking into account the contribution to the THG rising from the dielectric inclusion in the structure. We have suggested that in order to separate the THG arose from the metal from that generated in the dielectric, the latter should be etched several nanometers under the wires. We have introduced an alternative way to experimentally investigate this model. As the effective $\chi^{(3)}$ will depend on the distance of the nanowires and the film, this finding may be easily tested experimentally. The same concept can be applied to the case

of four-wave mixing or to the three-dimensional variant of the presented structure–the film-coupled nanocubes–which possess very similar resonances and even higher field enhancements, and it can be easily fabricated by using colloidal methods[18]. Our findings show a route to obtain efficient nonlinear processes that exceed other approaches by several orders of magnitude.

ACKNOWLEDGMENTS

We thank D. de Ceglia, M. A. Vincenti, and J. W. Haus for helpful input and discussion. This work was supported by the Air Force Office of Scientific Research (AFOSR, Grant No. FA9550-09-1-0562) and by the Army Research Office through a Multidisciplinary University Research Initiative (Grant No. W911NF-09-1-0539).

* cristian.ciraci@iit.it

[1] J. Haus, R. Inguva, and C. Bowden, Physical Review A **40**, 5729 (1989).
[2] I. Iorsh, P. Belov, A. Zharov, I. Shadrivov, and Y. Kivshar, Physical Review A **86**, 023819 (2012).
[3] R. S. Bennink, Y.-K. Yoon, R. W. Boyd, and J. E. Sipe, Optics Letters **24**, 1416 (1999).
[4] M. Larciprete, A. Belardini, M. Cappeddu, D. de Ceglia, M. Centini, E. Fazio, C. Sibilia, M. Bloemer, and M. Scalora, Physical Review A **77**, 013809 (2008).
[5] N. Katte, J. W. Haus, P. Powers, A. Sarangan, J. Gao, and M. Scalora, JOSA B **28**, 2277 (2011).
[6] R. Czaplicki, H. Husu, R. Siikanen, J. Mäkitalo, M. Kauranen, J. Laukkanen, J. Lehtolahti, and M. Kuittinen, Physical Review Letters **110**, 093902 (2013).
[7] B. K. Canfield, S. Kujala, K. Jefimovs, J. Turunen, and M. Kauranen, Optics Express **12**, 5418 (2004).
[8] M. W. Klein, C. Enkrich, M. Wegener, and S. Linden, Science **313**, 502 (2006).
[9] M. W. Klein, M. Wegener, N. Feth, and S. Linden, Optics Express **15**, 5238 (2006); **16**, 8055 (2008).
[10] C. Ciracì, E. Poutrina, M. Scalora, and D. R. Smith, Physical Review B **86**, 115451 (2012).
[11] A. R. Davoyan, I. V. Shadrivov, A. A. Zharov, D. K. Gramotnev, and Y. S. Kivshar, Physical Review Letters **105**, 116804 (2010).
[12] C. Argyropoulos, C. Ciracì, and D. R. Smith, Applied Physics Letters **104**, 063108 (2014).
[13] J. Renger, R. Quidant, N. van Hulst, and L. Novotny, Physical Review Letters **104**, 046803 (2010).
[14] J. Renger, R. Quidant, and L. Novotny, Optics Express **19**, 1777 (2011).
[15] G. A. Wurtz, R. Pollard, W. Hendren, G. P. Wiederrecht, D. J. Gosztola, V. A. Podolskiy, and A. V. Zayats, Nature Nanotechnology **6**, 107 (2011).
[16] N. Liu, M. Mesch, T. Weiss, M. Hentschel, and H. Giessen, Nano Letters **10**, 2342 (2010).
[17] N. Landy, S. Sajuyigbe, J. Mock, D. Smith, and W. Padilla, Physical Review Letters **100**, 207402 (2008).
[18] A. Moreau, C. Ciracì, J. J. Mock, R. T. Hill, Q. Wang, B. J. Wiley, A. Chilkoti, and D. R. Smith, Nature **492**, 86 (2012).
[19] C. Ciracì, R. Hill, J. J. Mock, and Y. A. Urzhumov, Science **337**, 1072 (2012).
[20] J. Zuloaga, E. Prodan, and P. Nordlander, Nano Letters **9**, 887 (2009).
[21] T. V. Teperik, P. Nordlander, J. Aizpurua, and A. G. Borisov, Physical Review Letters **110**, 263901 (2013).
[22] J. W. Haus, D. de Ceglia, M. A. Vincenti, and M. Scalora, Journal of the Optical Society of America B-Optical Physics **31**, A13 (2014).
[23] K. J. Savage, M. M. Hawkeye, R. Esteban, and A. G. Borisov, Nature **491**, 574 (2012).
[24] J. A. Scholl, A. García-Etxarri, A. L. Koh, and J. A. Dionne, Nano Letters **13**, 564 (2013).
[25] G. Hajisalem, M. S. Nezami, and R. Gordon, Nano Letters (2014).
[26] X. Chen, C. Ciracì, D. R. Smith, and S.-H. Oh, Nano Letters **15**, 107–113 (2015).
[27] J. B. Lassiter, X. Chen, X. Liu, C. Ciracì, T. B. Hoang, S. Larouche, S.-H. Oh, M. H. Mikkelsen, and D. R. Smith, ACS Photonics **1**, 1212 (2014).
[28] K. Li, X. Li, D. Y. Lei, S. Wu, and Y. Zhan, Applied Physics Letters **104**, 261105 (2014).
[29] M. Scalora, M. A. Vincenti, D. de Ceglia, and J. W. Haus, Physical Review A **90**, 013831 (2014).
[30] N. D. Lang and W. Kohn, Physical Review B **3**, 1215 (1971).
[31] N. Lang and W. Kohn, Physical Review B **7**, 3541 (1973).
[32] A. Liebsch, Physical Review B **48**, 11317 (1993).
[33] J. Tiggesbäumker, L. Köller, and K. H. Meiwes-Broer, Physical Review A **48**, R1749 (1993).
[34] J. Lermé, B. Palpant, B. Prével, M. Pellarin, M. Treilleux, J. Vialle, A. Perez, and M. Broyer, Physical Review Letters **80**, 5105 (1998).
[35] C. Ciracì, J. B. Pendry, and D. R. Smith, ChemPhysChem **14**, 1109 (2013).
[36] R. W. Boyd, *Nonlinear Optics* (Academic Press, San Diego, 2006).
[37] Comsol Multiphysics, `http://www.comsol.com/`.
[38] A. Moreau, C. Ciracì, and D. R. Smith, Physical Review B **87**, 045401 (2013).
[39] P. B. Johnson and R. W. Christy, Physical Review B **6**, 4370 (1972).
[40] C. Ciracì, X. Chen, J. J. Mock, F. McGuire, X. Liu, S.-H. Oh, and D. R. Smith, Applied Physics Letters **104**, 023109 (2014).
[41] J. B. Lassiter, F. McGuire, J. J. Mock, C. Ciracì, R. T. Hill, B. J. Wiley, A. Chilkoti, and D. R. Smith, Nano Letters **13**, 5866 (2013).
[42] J. Mcmahon, S. Gray, and G. Schatz, Physical Review B **82**, 035423 (2010).
[43] G. Toscano, C. Rockstuhl, F. Evers, H. Xu, N. A. Mortensen, and M. Wubs, arXiv.org (2014), 1408.5862v1.